



HAL
open science

Characterization of Atmospheric Ekman Spirals at Dome C, Antarctica

Jean-François Rysman, Alain Lahellec, Etienne Vignon, Christophe Genthon,
Sébastien Verrier

► **To cite this version:**

Jean-François Rysman, Alain Lahellec, Etienne Vignon, Christophe Genthon, Sébastien Verrier. Characterization of Atmospheric Ekman Spirals at Dome C, Antarctica. *Boundary-Layer Meteorology*, 2016, 160 (2), pp. 363-373. 10.1007/s10546-016-0144-y . hal-01306757

HAL Id: hal-01306757

<https://hal.sorbonne-universite.fr/hal-01306757>

Submitted on 25 Apr 2016

HAL is a multi-disciplinary open access archive for the deposit and dissemination of scientific research documents, whether they are published or not. The documents may come from teaching and research institutions in France or abroad, or from public or private research centers.

L'archive ouverte pluridisciplinaire **HAL**, est destinée au dépôt et à la diffusion de documents scientifiques de niveau recherche, publiés ou non, émanant des établissements d'enseignement et de recherche français ou étrangers, des laboratoires publics ou privés.

1 Characterization of atmospheric Ekman spirals at Dome C, Antarctica

2 **Jean-François Rysman · Alain Lahellec · Etienne**

3 **Vignon · Christophe Genthon · Sébastien Verrier**

4

5 **Abstract** We use wind speed and temperature measurements taken along a 45-m meteorological tower
6 located at Dome C, Antarctica (75.06 °S, 123.19 °E) to highlight and characterize the Ekman spiral.
7 Firstly, temperature records reveal that the atmospheric boundary layer at Dome C is stable during
8 winter and summer nights (i.e., > 85 % of the time). The wind vector also shows a strong dependence
9 in speed and direction with elevation. The Ekman model was then fitted to the measurements. Results
10 show that the wind vector followed the Ekman spiral structure for more than 20 % of the year 2009. Most
11 Ekman spirals have been detected during summer nights, that is, when the boundary layer is slightly
12 stratified. During these episodes, the boundary-layer height ranged from 25 to 100 m, eddy viscosity
13 coefficient from 0.004 to 0.06 m² s⁻¹, and the Richardson number from 0 to 1.6.

14 **Keywords** Atmospheric boundary layer · Dome C · Ekman spiral · Meteorological tower

15 1 Introduction

16 The Antarctic plateau is the coldest and one of the driest places on Earth (King and Turner, 1997).
17 The flatness of this ice-covered desert with altitude ranging from 2000 to 4000 m, along with its extreme
18 climatic conditions, makes it an exceptional setting for meteorological observations, particularly for the
19 study of the atmospheric boundary layer. The Antarctic Plateau boundary layer is extremely stable
20 and shallow during a large part of the year (Connolley, 1996; Hudson and Brandt, 2005; Hagelin et al.,

JF Rysman

Laboratoire de Météorologie Dynamique, IPSL, CNRS, Ecole Polytechnique, France E-mail: jfrysman@lmd.polytechnique.fr

A Lahellec

Laboratoire de Météorologie Dynamique, IPSL, UPMC Univ. Paris 06, France

E Vignon

Université Grenoble Alpes / CNRS Laboratoire de Glaciologie et Géophysique de l'Environnement (LGGE), France

C Genthon

Université Grenoble Alpes / CNRS Laboratoire de Glaciologie et Géophysique de l'Environnement (LGGE), France

S Verrier

LOCEAN (UPMC/IPSL), CNES, France

21 2008; Genthon et al., 2013) but can be convective on summer days, e.g., at Dome C (Mastrantonio
22 et al., 1999; Georgiadis et al., 2002; Argentini et al., 2005; King et al., 2006; Genthon et al., 2010;
23 Pietroni et al., 2012; Casasanta et al., 2014). Yet, because of the extreme conditions encountered in
24 Antarctica, long-term and steady measurements are rare and the Antarctic Plateau boundary layer is
25 still not yet fully characterized and understood (i.e., the role of the Coriolis effect in very stable regimes,
26 the parametrization and modelling of the long-lived stable boundary layer in winter (Pietroni et al.,
27 2012)).

28 One consequence of a neutral or stable boundary layer is the dependence of wind speed and direction
29 on the elevation. Ekman (1905) developed, initially for the oceanic boundary layer and then adapted
30 to the atmosphere, a theoretical model to explain the vertical wind profile. Specifically, Ekman (1905)
31 showed that, in a neutral boundary layer, flow is constrained by pressure forces, Coriolis forces, and
32 the divergence of turbulent fluxes of momentum resulting in the well-known Ekman spiral. However,
33 the conditions for Ekman spirals (no baroclinicity, no topographic effects, steady state, static neutrality
34 and no subsidence) are very seldom met in the atmosphere, although they are frequent in the ocean.
35 As a result, very little evidence of the Ekman spiral has emerged for the atmosphere, e.g., at Leipzig
36 (Germany) (Mildner, 1950; Lettau, 1950), at Cabauw (the Netherlands) (Van Ulden and Wieringa, 1996),
37 in the Arctic (Grachev et al., 2005), and in Antarctica (Mahrt and Schwerdtfeger, 1970; Kuhn et al.,
38 1977; Lettau et al., 1977; Kottmeier, 1986). More recently, Genthon et al. (2010) mentioned the night
39 time occurrences of the Ekman spiral at Dome C on the Antarctic plateau, this location meeting the
40 conditions for the frequent occurrence of Ekman spirals. Indeed, the Dome C is located on a very flat
41 plateau with a slope $< 1 \times 10^{-3}$. This region is isolated and rarely affected by atmospheric perturbations,
42 allowing a steady-state and barotropic atmosphere, with summer nights favorable to neutral or slightly
43 stratified boundary layers. Finally, very few attempts to estimate the subsidence at Dome C has been
44 done so far (Argentini et al., 2005; Pietroni et al., 2012) and the occurrence and intensity of subsidence
45 at Dome C is still an open question.

46 The observation and characterization of the atmospheric Ekman spiral around the world are worth-
47 while in terms of evaluating the turbulence parametrizations of climate models. Indeed, Sandu et al.
48 (2014) and Holtslag et al. (2013) describe the current problem of modelling the stable boundary layer,
49 showing a global tendency of models to both overestimate the surface drag that leads to an excessively
50 deep boundary layer, and to underestimate wind rotation with height in the lower atmosphere. Therefore
51 our study aims at providing a detailed characterization of the Ekman spiral at Dome C, including the
52 estimation of the eddy viscosity coefficient. To this aim, we used wind and temperature observations
53 collected between January and December 2009 at a meteorological tower located at Dome C.

54 Section 2 presents the geographical settings of Dome C and the characteristics of the measurements,
 55 with the Ekman model and method of analysis presented in Sect. 3. Section 4 is dedicated to the results.
 56 Firstly, we characterize the atmospheric stability at Dome C that results in the strong vertical dependence
 57 of the wind vector. We then identify conditions under which the Ekman model fitted the wind profiles
 58 in 2009 before evaluating and discussing the associated parameters. The discussion is found in Sect. 5.

59 2 Geographical settings and measurements

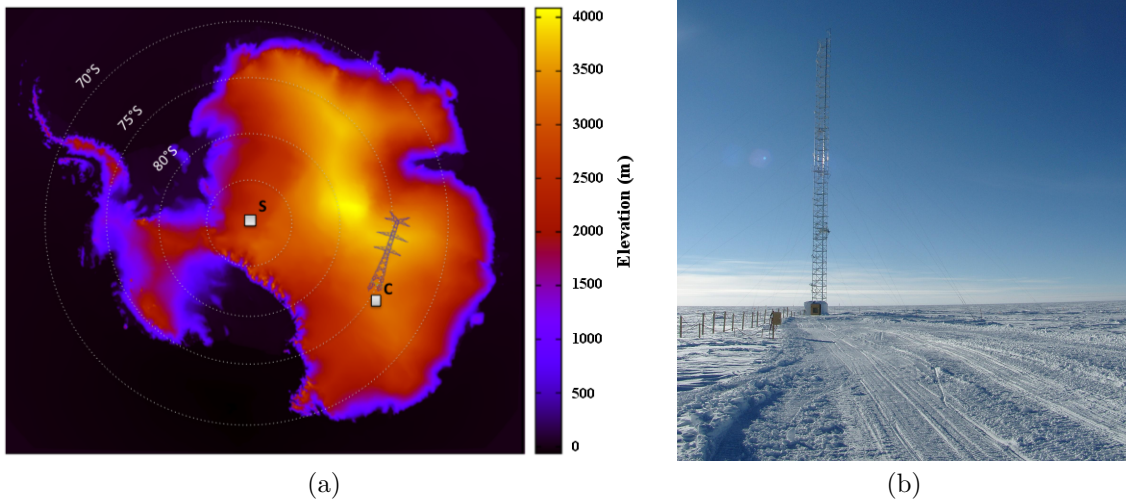


Fig. 1 (a) Map of Antarctica and the 45-m tower location (C): S symbolises the South Pole. (b) The instrumented tower.

60 Dome C is a local topographic maximum ($75^{\circ} 06' S$, $123^{\circ} 20' E$, 3233 m a.s.l.) of the Antarctic
 61 Plateau where the French-Italian Concordia scientific station has operated since 1997 (Fig. 1a). A 45-m
 62 meteorological tower was erected close to the station (Fig. 1b) on which temperature, humidity and
 63 wind measurements have been taken since 2008. In particular, in 2009, six Vaisälä thermo-hygrometers
 64 (four HMP155 and two HMP45AC), six platinum resistance thermometers in mechanically ventilated
 65 shields and six Young 45106 aerovanes were operated at heights of 3.6 m, 11 m, 18.6 m, 25.9 m, 33.2 m
 66 and 42.4 m (± 0.5 m). Measurements were taken with a 10-second timestep and averaged over 30 min.
 67 These measurements have already provided new insights into the Antarctic boundary layer (Genthon
 68 et al., 2010, 2013; Barral et al., 2014; Rysman et al., 2015).

69 3 Ekman spiral

70 3.1 The Ekman model

71 In the Ekman model, the wind vector rotates and increases in magnitude with elevation showing a
72 spiral shape on the wind hodograph known as the Ekman spiral. The Ekman spiral results from the
73 equilibrium between pressure forces, Coriolis forces and the divergence of turbulent fluxes of momentum.
74 Theoretically, above a given height, the flow follows the large-scale atmospheric circulation. The Ekman
75 model equations can be expressed as follows,

$$76 \quad k_m \frac{\partial^2 \bar{u}}{\partial z^2} + f(\bar{v} - \bar{v}_g) = 0, \quad (1a)$$

$$k_m \frac{\partial^2 \bar{v}}{\partial z^2} - f(\bar{u} - \bar{u}_g) = 0, \quad (1b)$$

77 where f is the Coriolis parameter, k_m is the eddy viscosity coefficient taken to be constant vertically, u
78 and v are the horizontal wind components within the boundary layer, and u_g and v_g are the large-scale
79 wind components; the overbar corresponds to Reynolds averaging (see Holton (1992) for details). The
80 wind components for the Southern Hemisphere are thus,

$$81 \quad u = -u_g \cos(\gamma z) e^{-\gamma z} + v_g \sin(\gamma z) e^{-\gamma z} + u_g, \quad (2a)$$

$$82 \quad v = -v_g \cos(\gamma z) e^{-\gamma z} - u_g \sin(\gamma z) e^{-\gamma z} + v_g, \quad (2b)$$

83 where $\gamma = (-f/2k_m)^{1/2}$. The Ekman height is usually defined as $h_{ek} = \pi/\gamma$ (Holton, 1992) and cor-
84 responds to the distance from the ground where surface drag becomes negligible. Use of the Ekman
85 model to fit the measurements allows one to characterize the eddy viscosity coefficient, the large-scale
86 wind and the boundary-layer height. Note that, as the eddy viscosity coefficient is height dependant in
87 a stratified boundary layer, the Ekman model only fits wind profiles when the k_m coefficient does not
88 vary significantly along the tower; the k_m value is thus an average value along the vertical.

89 3.2 Model fitting

90 To assess the validity of the Ekman model for characterizing the wind profile at Dome C, the Ekman
91 model was fitted to each 30-min averaged wind profile using Eq. 2. The large-scale wind components
92 were constrained to the $[-20:20]$ m s⁻¹ range. Moreover, as the accuracy of wind sensors is 0.3 m s⁻¹,
93 we only retained wind measurements with speed exceeding 1 m.s⁻¹ and ensured that at least four levels
94 out of the available six met this requirement. The γ parameter range was set to take into account the

95 angular accuracy of the wind aero-vanes and constrained to [0.004:0.13], this constraint implies that the
 96 lowest Ekman height characterized by the tower is 24 m. The non-linear fitting has been performed using
 97 the Levenberg-Marquardt algorithm (Levenberg et al., 1944).

98 Assessing whether the Ekman model fits the measurements implies testing the consistency of several
 99 well-chosen variables with the expected probability distribution. In particular, we tested the residuals
 100 (r) (not shown in the following) and the quadratic error (Q^2) distributions. Residuals are thus defined
 101 as,

$$102 \quad r_i = y_i - f(x_i) \quad (3)$$

103 where $i = 1 \dots n$ is associated with n measurements (12 in our analysis), y is a dependant variable (e.g.,
 104 wind observation), f is the model function (e.g., Ekman model) and x is an independent (i.e., predictor)
 105 variable (e.g., altitude). The quadratic error is defined as,

$$106 \quad Q^2 = \sum_{i=1}^n \frac{r_i^2}{\sigma^2} \quad (4)$$

107 where σ is the standard deviation (wind sensor accuracy). The data are assumed to follow a normal
 108 distribution and to be centered on the Ekman model, while the measurement errors are assumed to be
 109 independent and Gaussian with a zero mean. If the Ekman model is relevant for describing the wind
 110 profile in the Dome C boundary layer, then our fitted Q^2 distribution should have a χ^2 distribution with
 111 nine degrees of freedom (12 measurements – three parameters). This hypothesis is tested by computing
 112 the χ^2 probabilities defined as,

$$113 \quad y = \int_{\chi^2}^{+\infty} \varphi(\chi'^2, n) d\chi'^2 \quad (5)$$

114 φ is a probability density function with n degrees of freedom, which follows a χ^2 distribution. If our
 115 fitted Q^2 distribution follows the χ^2 distribution with n degrees of freedom, then the y -distribution must
 116 be constant as a function of probability. To obtain such a distribution, the standard deviation has to be
 117 adjusted (see below).

118 4 Results

119 Figure 2 highlights the stability of the lower atmosphere at Dome C in 2009 (>85% of the year). From
 120 March to mid-October, the atmosphere is stable almost without interruption except during a period of
 121 sudden warming at the beginning of July. On some days (e.g., in early May) the stability is considerable,
 122 stratification exceeding 10 K between 42.4 m and 3.6 m. From January to February, and from November
 123 to December, the diurnal variability is large; the atmosphere is moderately stable at night and often

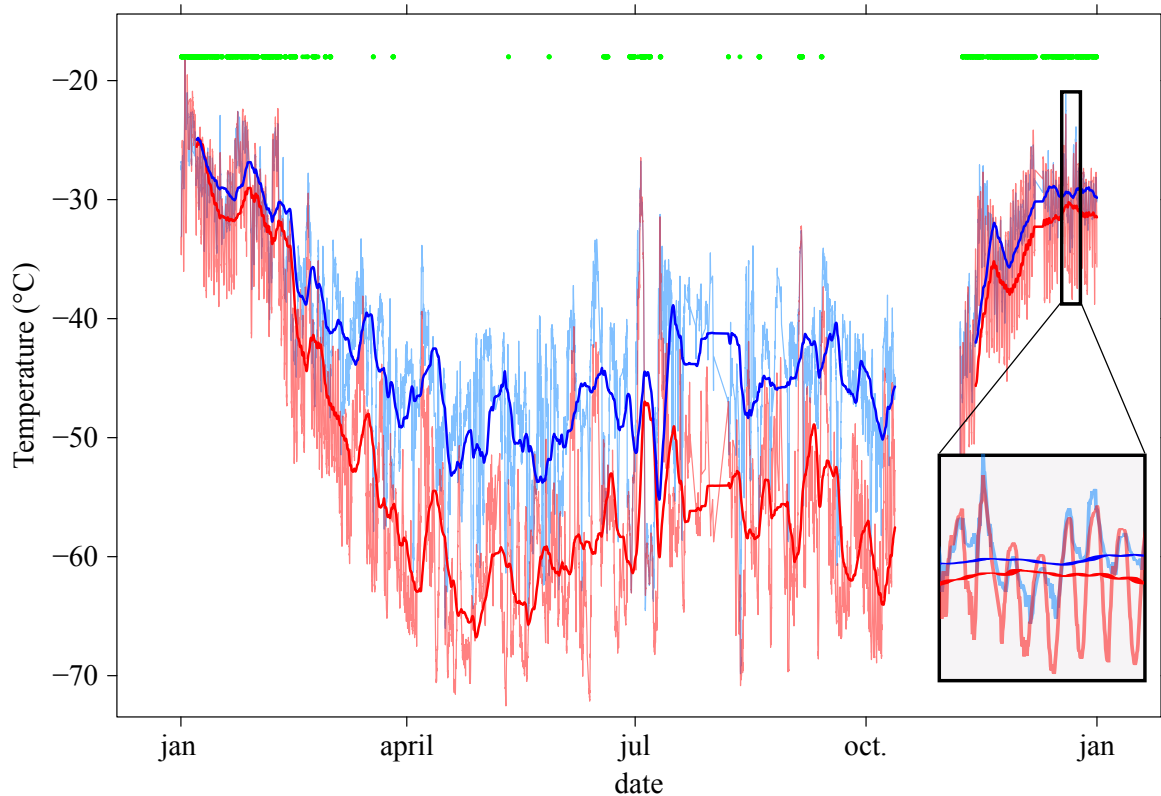


Fig. 2 Temperature for 3.6 m (shaded red) and 42.4 m (shaded blue) sensors in 2009. A six-day moving average temperature is displayed using red (3.6 m) and blue (42.4 m) lines. Green points indicate the episodes of convective boundary layer. A zoom is shown in the black box to highlight the diurnal cycle.

124 convective during the day. Further information about the seasonal cycle of temperature at Dome C can
 125 be found in Genthon et al. (2013).

126 During summer, wind speed and direction are almost independent of altitude during daytime —
 127 when the sun is sufficiently high above the horizon, that is, from approximately 0900Z to 1800Z — but
 128 when the sun is low above the horizon, the atmosphere becomes very stratified. Figure 3 shows the wind
 129 hodograph for a typical summer afternoon (24 December). At 1200Z and 1500Z, the wind direction does
 130 not depend on height while the wind speed is very slightly dependent on height. From 1800Z onwards, a
 131 strong height dependence in speed appears (from 2.8 m s^{-1} at 3.6 m to 4.3 m s^{-1} at 42.4 m) but without
 132 height dependence in direction. At 2100Z, the wind is markedly stratified in terms of both speed (from
 133 2.5 m s^{-1} at 3.6 m to 6.1 m s^{-1} at 42.4 m) and direction (from 46.5° at 3.6 m to 9.5° at 42.4 m). This
 134 stratification results in an Ekman spiral-like structure.

135 Therefore, since the atmosphere exhibited a neutral and stable temperature stratification at Dome C
 136 for more than 85 % of the calendar year 2009, with numerous wind observations showing a rotation and
 137 increase with height, we tested the validity of the Ekman model (Eq. 2). Firstly, as explained in Sect. 3.2,
 138 the standard deviation (i.e., the wind sensor accuracy provided by the manufacturer) was adjusted to

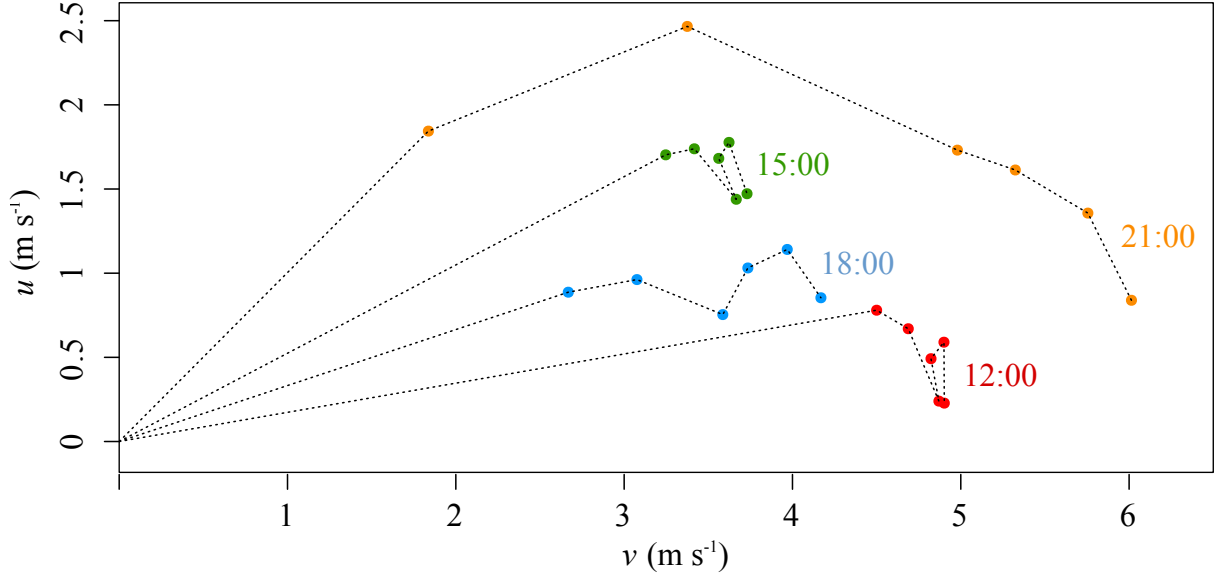


Fig. 3 Wind hodograph as a function of time on 24 December 2012.

139 obtain a constant y -distribution (Eq. 5). This showed that we needed to increase the standard deviation
 140 σ by a factor of 2.5 to account for the extreme climatic conditions of the Antarctic region as well as
 141 the turbulent wind fluctuations. Taking this correction into account, we found that during at least 20 %
 142 of the year 2009 (24 % of neutral and stable conditions), the wind profile followed an Ekman spiral
 143 pattern (Fig. 4). The vast majority of Ekman spirals were observed from January to mid-March, and
 144 from mid-November to December, i.e., approximately when the diurnal cycle is significant at Dome C.
 145 Fig. 2 shows that very few Ekman spirals are detected when the temperature is extremely low (especially
 146 from mid-April to the end of May), while several Ekman spirals are detected when the temperature is
 147 higher (e.g., in June).

148 Figure 5 highlights the occurrence of Ekman spirals and the corresponding Ekman-layer height in
 149 late December 2009. We also plotted the bulk Richardson number (R_i) between the highest and lowest
 150 levels of the tower, defined as,

$$151 \quad R_i = \frac{\frac{g}{\theta_v} \frac{\Delta \bar{\theta}_v}{\Delta z}}{\frac{\Delta \bar{U}^2}{\Delta z} + \frac{\Delta \bar{V}^2}{\Delta z}} \quad (6)$$

152 where θ_v is the virtual potential temperature. Figure 5 emphasises that the Ekman model fits the wind
 153 during the night, i.e., when the atmosphere is slightly stable and the Richardson number slightly positive.
 154 During these episodes, the Ekman height ranges from 30 to 60 m. Figure 5 also shows that, as the
 155 Richardson number increases during the night (associated with increasing temperature stratification),
 156 the Ekman height decreases. Moreover, this figure also highlights that when the Richardson number is
 157 high (>3), and thus when turbulence is confined very close to the surface, the wind profile does not
 158 present an Ekman spiral structure. Note that free convection and extreme stable stratification episodes

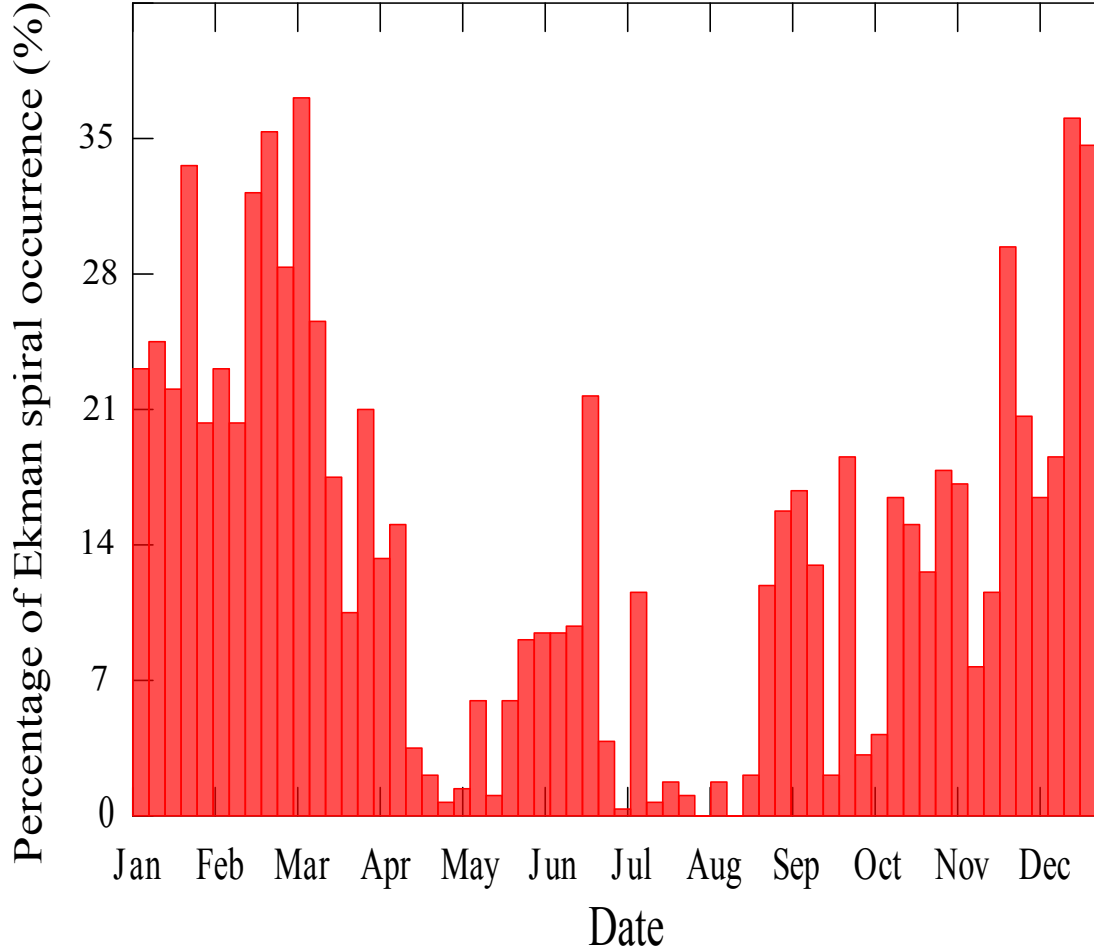


Fig. 4 Percentage Ekman spirals occurring over 6-day periods during the year 2009. 50% indicates that Ekman spirals occurred during half of a given 6-day period. Note the Ekman spiral structure cannot be detected with the tower when the atmospheric boundary layer depth is lower than 24 m.

159 highlighted by the negative and strongly positive values of R_i are associated to very small difference in
 160 temperature and/or in wind between top and bottom of the tower and are thus subject to high incertitude
 161 given the limited accuracy of wind and temperature sensors.

162 Figure 6 presents a normalized Ekman spiral i.e., $(\sqrt{u_g^2 + v_g^2} - \sqrt{v^2 + u^2})/\sqrt{u_g^2 + v_g^2}$ as a function
 163 of z/h_{ek} when the Ekman model fits the wind profiles. This figure shows that the 42.4-m sensor and
 164 even the 33.2-m sensor are sometimes found above the Ekman height. The normalized Ekman spiral also
 165 shows that the 18.6-m sensor sometimes show null wind speed and that the 3.6-m wind speed is, most
 166 of the time, over estimated by the Ekman model. Both features can also be observed in the analysis of
 167 residuals (not shown). It is not surprising that most of the time, the wind speed at 3.6 m is higher than
 168 the value predicted by the Ekman model because, close to the ground, in the atmospheric surface layer,
 169 the viscosity coefficient varies sharply when it is assumed constant in the Ekman model. This result
 170 supports the hypothesis that the surface-layer height lies between 3 and 10 m for the fitted case.

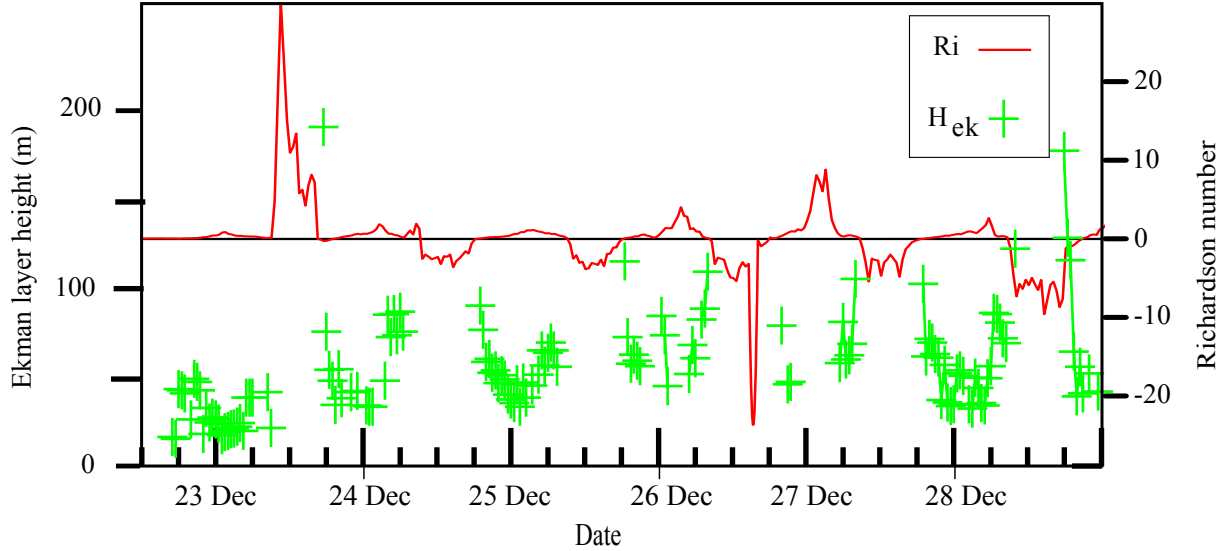


Fig. 5 Richardson number (red) and Ekman height (green) when the wind profile follows the Ekman spiral model. Note that free convection and extreme stable stratification episodes highlighted by the negative and strongly positive values of R_i are associated to very small difference in temperature and/or in wind between top and bottom of the tower and are thus subject to high incertitude given the limited accuracy of wind and temperature sensors.

171 When the Ekman model fits the wind profile (i.e., mainly during summer nights), the boundary-
 172 layer height mostly ranges between 25 and 100 m, which is in agreement with previous studies (King
 173 et al., 2006; Pietroni et al., 2012). This value can be placed into perspective since on convective days
 174 the boundary-layer height can reach 200-350 m (Aristidi et al., 2005; Argentini et al., 2005; King et al.,
 175 2006).

176 The eddy viscosity coefficient characterizes the transport and dissipation of energy in the flow. The fit
 177 shows that this coefficient mainly ranges between 0.004 and $0.06 \text{ m}^2 \text{ s}^{-1}$, that is, two orders of magnitude
 178 lower than the typical value at mid-latitudes for a stable layer. The Richardson number mostly ranges
 179 between zero and 1.6 when the wind profile follows the Ekman model, i.e., in a neutral or slightly stratified
 180 boundary layer.

181 5 Discussion and conclusion

182 We have highlighted and characterized a significant number of atmospheric Ekman spirals during the
 183 2009 campaign at Dome C, Antarctica. Specifically, we analyzed wind and temperature measurements
 184 using aero-vanes and thermometers deployed along a 45-m tower. We showed that the boundary layer
 185 was neutral or stable during 85 % of the year. Ekman spirals were detected for at least 20 % of the time
 186 series (i.e., more than 52 days in total) mainly during summer “nights” (i.e., with low solar elevation
 187 above the horizon). This analysis also revealed that the Ekman height mostly ranges between 25 and
 188 100 m, much shallower than for the mid-latitude boundary layer. We found that, when the Ekman model
 189 fits the wind profile, the eddy viscosity coefficient ranges between 0.004 and $0.06 \text{ m}^2 \text{ s}^{-1}$, while the bulk

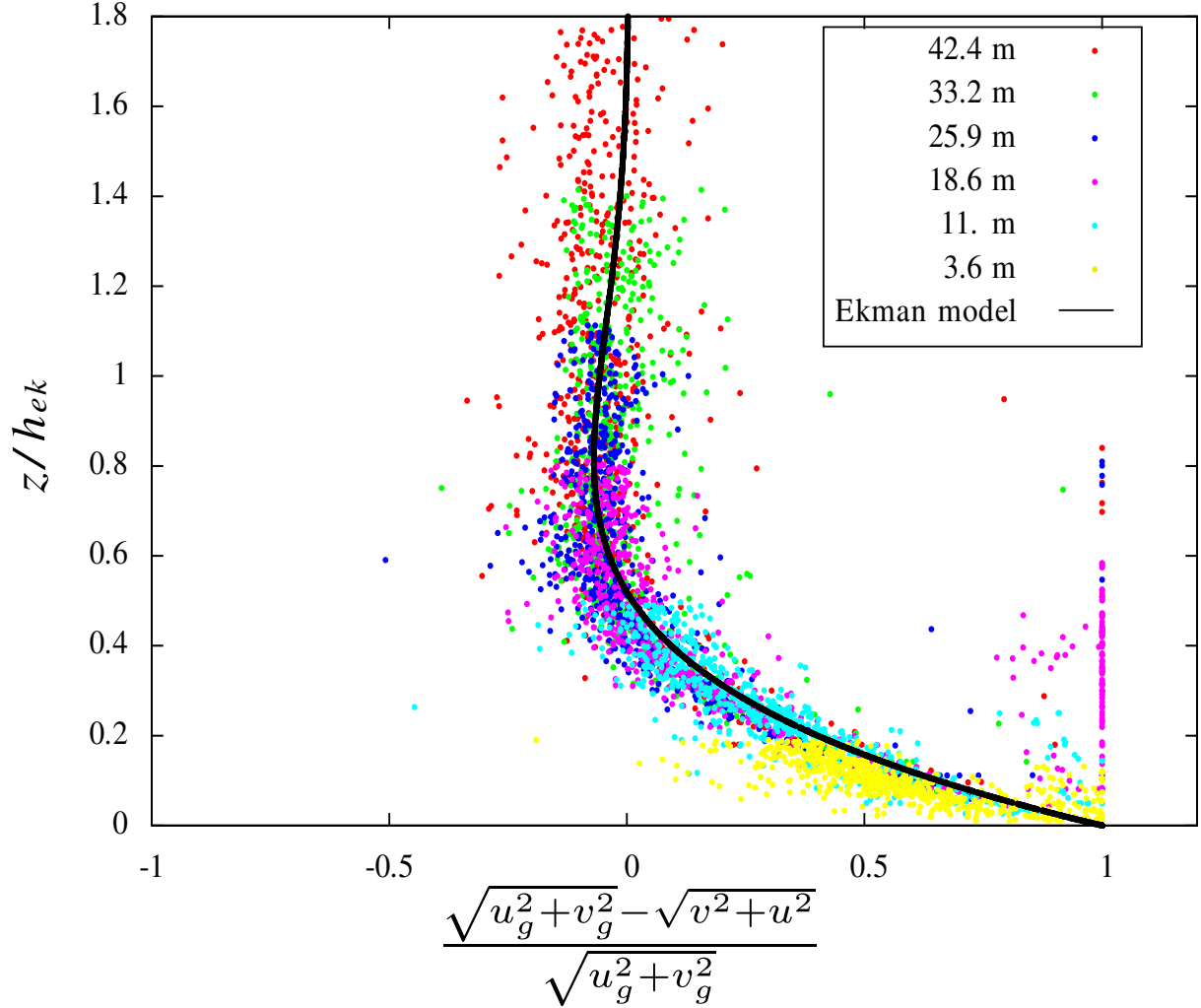


Fig. 6 Normalized Ekman spiral when the Ekman model fits the wind profiles per sensor. The thick black line shows the Ekman model relation.

190 Richardson number mainly ranges between zero and 1.6, implying that the boundary layer is neutral or
 191 slightly stratified.

192 Using measurements from a similar tower located on the Arctic sea-ice, Grachev et al. (2005) defined
 193 four regimes for the stable boundary layer that depend on the turbulence characteristics, the boundary
 194 layer stability and the influence of the Earth’s rotation. Our results show that, when the Ekman model
 195 fits the observations, the boundary layer is in the so-called “turbulent Ekman layer” regime (when
 196 $R_i \leq R_{ic} \approx 0.2$, where R_{ic} is the critical Richardson number) and in the “intermittently turbulent
 197 Ekman layer” regime (or supercritical stable regime) (when $R_i \geq R_{ic} \approx 0.2$). In complete accordance
 198 with our results, Grachev et al. (2005) argued that, for these regimes, the surface layer is very shallow and
 199 the wind profile is influenced by the Coriolis force, with some Ekman-spiral-like features being observed.
 200 Specific parametrizations associated with these regimes that take into account the Coriolis effect are
 201 certainly needed especially in models with coarse vertical resolution.

202 It must also be emphasized that nearly 80 % of wind profiles were not adjusted to the Ekman model.
203 In particular, we showed that the Ekman model fitted the data rarely in winter. Several explanations
204 can be put forward. First, the aero-vanes are rarely monitored in winter due to the harsh meteorological
205 conditions and thus the extreme temperatures and frost deposition affect measurement availability and
206 accuracy. Moreover, the reduced number of Ekman spiral detected in winter is also related to the very
207 strong stability often found during this season, in contradiction to the condition of static neutrality of
208 the Ekman model. This is consistent with the Richardson number lying between zero and 1.6 when the
209 Ekman model fits the wind profile measurements, implying that Ekman spirals only develop within a
210 “slightly” (regarding average stability conditions at Dome C) stratified boundary layer for which eddy
211 viscosity coefficient does not vary significantly along the vertical. Occasional meteorological events can
212 also prevent the development of Ekman spirals such as the occurrence of nocturnal jets (Gallée et al.,
213 2015b) or subsidence (Argentini et al., 2005; Pietroni et al., 2012). Last but not least, seasonal conditions
214 can prevent the tower from characterizing the boundary layer. In the winter, the boundary layer can be
215 too shallow (only few tens of metres, Pietroni et al. (2012); Gallée et al. (2015a)) to be characterized by
216 the tower (i.e., lower than 24 m (see Sect. 3.2)) while, in the summer, the boundary layer can be too
217 deep.

218 Overall, this analysis provides new insights into the characteristics of the boundary layer, which
219 could be used for model parametrizations (e.g., eddy viscosity and Ekman height). Pietroni et al. (2012)
220 stressed the difficulty of defining the boundary-layer height in stable cases because its definition is often
221 based on available measurements rather than on theory. Therefore, our method, with its clear physical
222 background, could be applied for neutral and slightly stratified boundary layers at Dome C. Moreover,
223 Pietroni et al. (2012) evaluated several boundary-layer height parametrizations at Dome C. They showed
224 that the one proposed in Zilitinkevich (2002); Zilitinkevich et al. (2007) is the most accurate estimation of
225 boundary-layer height at Dome C. In this parametrization, the boundary-layer height equals the Ekman-
226 layer height when the atmosphere is neutral (see Eq. 3 from Zilitinkevich et al., 2007). This highlights the
227 relevance of using Ekman model for estimating the boundary-layer height in neutral or slightly stratified
228 boundary layer at Dome C.

229 Further analyses using this and subsequent datasets are needed to estimate the Ekman pumping and
230 the associated subsidence. Moreover as the measurements at Dome C tower are still on-going, information
231 about the seasonal and inter-annual variability of the boundary layer will be available and could be used
232 to detect possible changes in climatic conditions at Dome C in the context of the global warming.

233 **Acknowledgements** We would like to thank Jean-Yves Grandpeix for his valuable help for the statistical analysis and
234 Chantal Claud for her support that allows to achieve this paper. Boundary layer observation and research at Dome C

235 were supported by the French Polar Institute (IPEV; CALVA program), the Institut National des Sciences de l'Univers
236 (Concordia and LEFE-CLAPA programs), the Observatoire des Sciences de l'Univers de Grenoble (OSUG) and the École
237 Doctorale 129 - Sciences de l'environnement. We would like to thank the two anonymous referees and the editors Evgeni
238 Fedorovich and John R. Garratt for their helpful comments, suggestions and editing.

239 **References**

- 240 Argentini S, Viola A, Sempreviva AM, Petenko I (2005) Summer boundary-layer height at the plateau
241 site of Dome C, Antarctica. *Boundary-Layer Meteorol* 115:409–422, DOI 10.1007/s10546-004-5643-6
- 242 Aristidi E, Agabi K, Azouit M, Fossat E, Vernin J, Travouillon T, Lawrence JS, Meyer C, Storey JWV,
243 Halter B, Roth WL, Walden V (2005) An analysis of temperatures and wind speeds above Dome C,
244 Antarctica. *Astron Astrophys* 430:739–746, DOI 10.1051/0004-6361:20041876
- 245 Barral H, Vignon E, Bazile E, Traullé O, Gallée H, Genthon C, Brun C, Couvreur F, Le Moigne P (2014)
246 Summer diurnal cycle at Dome C on the Antarctic Plateau. 21st Symposium on Boundary Layer and
247 Turbulence.
- 248 Casasanta G, Pietroni I, Petenko I, Argentini S (2014) Observed and modelled convective mixing-layer
249 height at Dome C, Antarctica. *Boundary-Layer Meteorol* 151:587–608, doi:0.1007/s10546-014-9907-5
- 250 Connolley WM (1996) The Antarctic temperature inversion. *Int J Climatol* 16:1333–1342
- 251 Ekman VW (1905) On the influence of the Earth's rotation on ocean currents. *Ark Mat Astron Fys*
252 2:1–53
- 253 Gallée H, Barral H, Vignon E, Genthon C (2015) A case study of a low level jet during OPALE. *Atmos*
254 *Chem Phys Discussion* 14:31,091–31,109, DOI 10.5194/acp-15-1-2015
- 255 Gallée H, Preunkert S, Argentini S, Frey MM, Genthon C, Jourdain B, Pietroni I, Casasanta G, Barral
256 H, Vignon E, Legrand M, Amory C (2015) Characterization of the boundary layer at Dome C (East
257 Antarctica) during the OPALE summer campaign. *Atmos Chem Phys* 15:6225–6236, DOI 10.5194/acp-
258 15-6225-2015
- 259 Genthon C, Town MS, Six D, Favier V, Argentini S, Pellegrini A (2010) Meteorological atmospheric
260 boundary layer measurements and ECMWF analyses during summer at Dome C, Antarctica. *J Geo-*
261 *phys Res Atmos* 115:D05104, DOI 10.1029/2009JD012741
- 262 Genthon C, Gallée H, Six D, Grigioni P, Pellegrini A (2013) Two years of atmospheric boundary layer
263 observation on a 45-m tower at Dome C on the Antarctic plateau. *J Geophys Res Atmos* pp 3218–3232,
264 DOI 10.1002/jgrd.50128
- 265 Georgiadis T, Argentini S, Mastrantonio G, Sozzi AVR, Nardino M (2002) Boundary layer convective-like
266 activity at Dome Concordia, Antarctica. *Nuovo Cimento C Geophysics Space Physics C* 25:425

267 Grachev AA, Fairall CW, Persson POG, Andreas EL, Guest PS (2005) Stable boundary-layer scaling
268 regimes: The Sheba data. *Boundary-Layer Meteorol* 116:201–235, DOI 10.1007/s10546-004-2729-0

269 Hagelin S, Masciadri E, Lascaux F, Stoesz J (2008) Comparison of the atmosphere above the South Pole,
270 Dome C and Dome A: first attempt. *Mon Not R Astron Soc* 1510:1499–1510, DOI 10.1111/j.1365-
271 2966.2008.13361.x

272 Holton J (1992) *An introduction to dynamic meteorology*, Academic Press, San Diego, U.S.A, 511 pp.

273 Holtlag AAM, Svensson G, Baas P, Basu S, Beare B, Beljaars ACM, Bosveld FC, Cuxart J, Lindvall
274 J, Steeneveld GJ, Tjernström M, Van de Wiel BJH (2013) Stable boundary layers and diurnal cycles.
275 *Bull Amer Meteorol Soc* 94:1691–1706

276 Hudson SR, Brandt RE (2005) A Look at the Surface-Based Temperature Inversion on the Antarctic
277 Plateau. *J Clim* 18:1673–1696, DOI 10.1175/JCLI3360.1

278 King JC, Turner J (1997) *Antarctic meteorology and climatology*. Cambridge University Press, UK, 409
279 pp

280 King JC, Argentini SA, Anderson PS (2006) Contrasts between the summertime surface energy balance
281 and boundary layer structure at Dome C and Halley stations, Antarctica. *J Geophys Res Atmos*
282 111:D02105, DOI 10.1029/2005JD006130

283 Kottmeier C (1986) Shallow gravity flows over the Ekström ice shelf. *Boundary-Layer Meteorol.* 35(1-
284 2):1–20

285 Kuhn, M., Lettau, H., and Riordan, A. J. (1977) Stability Wind Spiraling in the Lowest 32 meters. in
286 *Meteorological Studies at Plateau Station, Antarctica; Pap. 7, Antarctic Res. Ser. 25, 93-1 I I.*

287 Lettau, H. (1950) A reexamination of the “Leipzig wind profile” considering some relations between wind
288 and turbulence in the frictional layer. *Tellus*, 2(2), 125–129.

289 Lettau, H., Riordan, A., Kuhn, M. (1977). Air temperature and two-dimensional wind profiles in the
290 lowest 32 meters as a function of bulk stability. *Meteorological studies at Plateau station, Antarctica,*
291 J. A. Businger, Ed., *Antarctic Research Series, Vol. 25, Amer. Geophys. Union, 77–91*

292 Levenberg, Kenneth (1944) A method for the solution of certain non-linear problems in least squares.
293 *Quarterly of applied mathematics*, 2: 164–168

294 Mahrt L, Schwerdtfeger W (1970) Ekman spirals for exponential thermal wind. *Boundary-Layer Meteorol*
295 1(2):137–145

296 Mastrantonio G, Malvestuto V, Argentini S, Georgiadis T, Viola A (1999) Evidence of a convective
297 boundary layer developing on the Antarctic plateau during the summer. *Meteorol Atmos Phys* 71:127–
298 132, DOI 10.1007/s007030050050

299 Mildner, P. (1932) Über die Reibung in einer speziellen Luftmasse in den untersten Schichten der Atmo-
300 sphäre. *Beitr Phys freien Atmosphäre.* 19:151–158.

301 Pietroni I, Argentini S, Petenko I, Sozzi R (2012) Measurements and parametrizations of the atmo-
302 spheric boundary-layer height at Dome C, Antarctica. *Boundary-Layer Meteorol* 143:189–206, DOI
303 10.1007/s10546-011-9675-4

304 Rysman JF, Verrier S, Lahellec A, Genthon C (2015) Analysis of boundary-layer statistical properties
305 at Dome C, Antarctica. *Boundary-Layer Meteorol* pp 1–11

306 Sandu I, Beljaars A, Balsamo G (2014) Improving the representation of stable boundary layers. *ECMWF*
307 *Newsletter* 138:24–31

308 Van Ulden A, Wieringa J (1996) Atmospheric boundary layer research at Cabauw. In: *Boundary-Layer*
309 *Meteorol* 78:34–69

310 Zilitinkevich SS (2002) Third-order transport due to internal waves and non-local turbulence in the stably
311 stratified surface layer. *QJR Meteorol Soc* 128(581):913–925

312 Zilitinkevich S, Esau I, Baklanov A (2007) Further comments on the equilibrium height of neutral and
313 stable planetary boundary layers. *QJR Meteorol Soc* 133:265–271.